



# Process optimization of dye-sensitized solar cells using TiO<sub>2</sub>–graphene nanocomposites

BULKESH SIWACH<sup>1,\*</sup>, DEVENDRA MOHAN<sup>1</sup>, SUNITA SHARMA<sup>2</sup> and DIVYA JYOTI<sup>3</sup>

<sup>1</sup>Laser Laboratory, Department of Physics, Guru Jambheshwar University of Science and Technology, Hisar 125001, India

<sup>2</sup>Department of Applied Science, The NorthCap University, Gurgaon 122017, India

<sup>3</sup>Department of Physics, University College, Faridkot 151202, India

\*Author for correspondence (bulkesh.siwach@gmail.com)

MS received 8 December 2016; accepted 14 March 2017; published online 23 November 2017

**Abstract.** TiO<sub>2</sub>–graphene (TGR) nanocomposites with varying concentrations of graphene from 0 to 1 wt% were prepared by direct mix method. X-ray diffraction (XRD) spectra confirmed the incorporation of graphene in photoanode material, which was further supported by field emission scanning electron microscopy (FESEM) and energy dispersive X-ray (EDX). The UV–visible spectrum of these nanocomposites shifted towards higher wavelength region as compared to pure TiO<sub>2</sub> that indicated a reduced band gap and hence, enhanced absorption bandwidth. Significant reduction in electron–hole recombination was confirmed from photoluminescence spectroscopy. These TGR nanocomposite films after tethering with black dye were employed as photoanodes in dye-sensitized solar cells (DSSCs). The efficiency of solar cells at varying concentrations of graphene (in photoanodes) was also investigated. TGR 0.25 wt% nanocomposite showed the highest photocurrent density ( $J_{SC}$ ) of 18.4 mA cm<sup>-2</sup> and efficiency ( $\eta$ ) of 4.69%.

**Keywords.** TiO<sub>2</sub>; graphene; nanocomposites; DSSCs; photoanode.

## 1. Introduction

Semiconductor-based solar cells such as silicon-based p–n junction solar cells have attracted an enormous attention as clean and abundant energy resources among all renewable energy sources. Although semiconductor-based solar cells have many limitations, for instance, high manufacturing cost and waste produced in the production process that causes environmental hazardous. Dye-sensitized solar cells (DSSCs) have been investigated as low cost next-generation photovoltaic devices due to their promising potential for high efficiency, eco-friendly production and low manufacturing costs, straightforward structural design as compared to conventional inorganic devices [1–6]. A typical DSSC device is made up of a photoanode on the surface of which, a sensitizer dye is attached, iodine-based redox-coupled electrolyte and a counter electrode of transparent conducting oxide (TCO) glass covered with a platinum film. The photoanode is a wide band gap semiconductor film coated on TCO glass substrate [7]. Till date, 11% conversion efficiency is attained [4], but research is continued to improve it further. The challenge in this device is the improved passage of photogenerated electrons across semiconductor nanoparticle film that competes with the charge recombination. To facilitate the transportation and suppress the recombination, there are numerous strategies including: (a) composite metal oxides with different band gaps as the semiconductors [8]; (b) the porous arrangement

directed perpendicular to the substrate [9–11]; as well as (c) introduction of charge carriers such as one-dimensional (1D) and two-dimensional (2D) nanomaterials to direct photogenerated electrons [12,13].

Graphene is a 2D material that exhibits good mechanical, optical, thermal and electrical properties and has really encouraged immense concern in designing novel graphene-based materials for a range of technological applications such as nanoelectronics, H<sub>2</sub> production and storage biosensing, polymer composites, drug delivery, intercalation materials and supercapacitors [14–18]. In recent times, graphene-based composite materials have prompted more interest than 1D composites due to the synergistic role of two or more functional components and many future applications [19]. Presently, titanium dioxide (TiO<sub>2</sub>) is abundant, nontoxic, most explored functional material and commercially inexpensive photocatalyst, as well as it is extensively used in organic transformations to fine chemicals and degradation of environmental pollutants in air as well as in water [20–23]. The photocatalysis of TiO<sub>2</sub> facilitates the quick recombination of electrons and holes. Also, its wide band gap of 3.2 eV limits its relevance to the ultraviolet (UV) region that constitutes merely a small portion (~ 5%) of the whole solar spectrum reaching the earth's surface [11]. Therefore, to consume irradiation from sunlight or from any artificial room light sources, the improvement of visible light-active TiO<sub>2</sub> is essential. A suitable

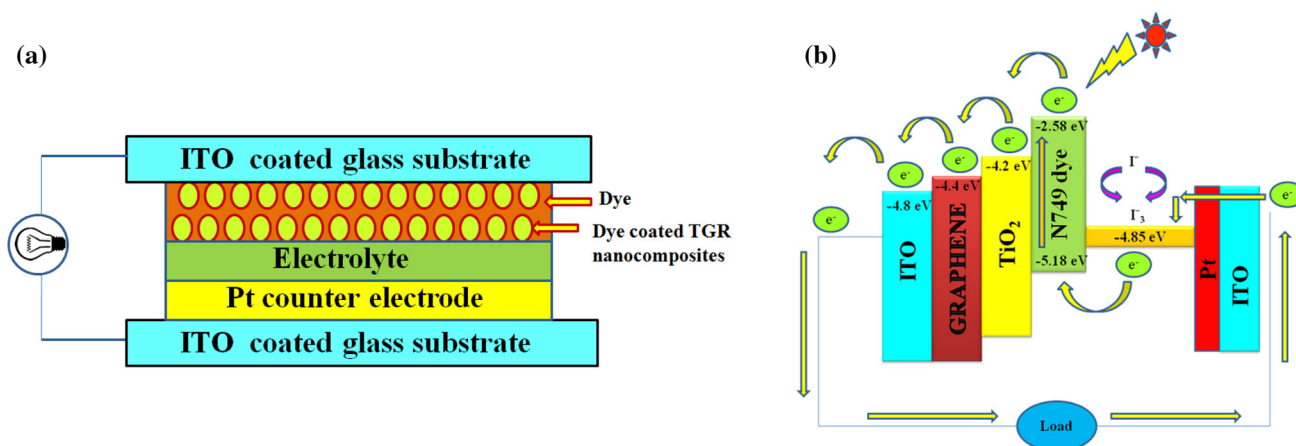


**Figure 1.** (a) Schematics of TGR-based DSSCs. (b) Typical energy levels of various components of TGR-based DSSCs employing an iodide/triiodide-based redox electrolyte and N749 as a sensitizer.

combination of graphene and  $\text{TiO}_2$  would provide a hybrid nanocomposite that combines enviable characteristics of respective nanoscaled building blocks for particular application. The use of graphene sheets inside DSSCs is very promising due to high mobility of structural layers and their electrochemical activities [12]. Graphene is a zero band gap material, but its band gap can be tailored [24]. Hence, graphene sheets can be mixed with  $\text{TiO}_2$  semiconductor to build a composite film to expect improved electron transport from  $\text{TiO}_2$  to a photoelectrode. TGR nanocomposites are found to be strictly different and more beneficial as a photocatalyst than other  $\text{TiO}_2$ -carbon composites and have become an excellent choice to overcome the recombination process and enhance the electron transfer. Nanocrystalline  $\text{TiO}_2$  attached closely on the graphene flake is possible to make graphene bridges, therefore, to reduce the  $\text{TiO}_2$ - $\text{TiO}_2$  links [2,25,26]. These surprising electronic properties succeed graphene for applications in prospect of optoelectronic devices [6,27].

In the present work, TGR nanocomposites with varying concentrations of graphene from 0 to 1 wt% are synthesized and their performance as photoanode materials in DSSCs are investigated. Platinum (Pt)-coated indium tin oxide (ITO) was used as counter electrode along with iodide-based electrolyte and black dye as sensitizer to design these cells.

## 2. Experimental

### 2.1 Materials

$\text{TiO}_2$  nanopowder, graphene, black dye and ITO glass ( $15 \Omega \text{sq}^{-1}$ ) were procured from Sigma Aldrich (USA). Polyethylene glycol (PEG<sub>20000</sub>) was purchased from Himedia (India). Deionized water was used throughout the experiments to minimize contamination. All the chemicals were used without any further purification unless otherwise stated.

### 2.2 Fabrication of TGR nanocomposite photoanodes

In an ultrasonic bath, ITO-coated glass substrates of adequate ( $2.5 \times 2.5 \text{cm}^2$ ) size were subjected, respectively, to acetone, ethanol and deionized water for 30 min for proper cleaning. Then, the substrates were dried under nitrogen flow and then masked by using scotch tape to decide the active area to deposit the films of TGR nanocomposites. Graphene powder,  $\text{TiO}_2$  nanopowder, deionized water and PEG<sub>20000</sub> were grounded together in a pestle for one and half hour to get a fine viscous paste. TGR nanocomposites from 0 to 1 wt% films were coated on conducting side of ITO by doctor-blade method. The films were dried at room temperature for 10 min, and subsequently annealed in a temperature-controlled furnace at  $450^\circ\text{C}$  for 30 min. These photoanodes were further immersed in 0.5 mM ethanolic solution of N749 (black dye) for 24 h and excess dye molecules were washed with ethanol.

### 2.3 Assembling and working principle of DSSC

The solar cells were assembled in a sandwich-type structure by placing the photoanodes on the top of Pt-coated counter electrodes. Figure 1a and b presents the schematics and the energy level diagram of the DSSC made with TGR nanocomposite photoanodes, respectively. Scotch tape was used as a spacer between the two electrodes of the cell. Iodide-based liquid electrolyte was injected into the devices by capillary force. When DSSC is illuminated under simulated light, electrons from the photoexcited dye are transported to the conduction band (CB) of  $\text{TiO}_2$  and then, transferred to ITO through the CB of graphene. It causes the oxidation of photosensitizer dye that gets regenerated by capturing electron from  $\text{I}^-$  ion of redox mediator. Now, this  $\text{I}^-$  ion is oxidized to  $\text{I}_3^-$ , transporting the positive charges to the counter electrode of DSSC. Therefore, in TGR-based DSSC; CB of graphene creates an additional path for electron transportation in addition to the traditional path. Also, due to good electrical conduction

of graphene, the graphene layer behaves as a channel for rapid transfer of photoexcited electrons. Therefore, the incorporation of graphene in the photoanode of DSSC acts as a bridge that enhances the interfacial electron transfer process by capturing electrons from the CB of  $\text{TiO}_2$ . This results in the increase in lifetime of the holes thereby suppressing the electron–hole recombination [28].

#### 2.4 Characterization techniques

The structure, morphology and composition of nanocomposite photoanode (without dye) films were revealed by the X-ray diffraction (XRD) from Rikagu Table-Top X-ray diffractometer, field emission scanning electron microscopy (FESEM) using TESCAN (model MIRA II LMH), energy dispersive X-ray (EDX) from INCA Penta FET  $\times 3$  attached with FESEM. Optical properties of these nanocomposite films were analysed by means of UV–visible absorbance using Varian UV–Vis spectrophotometer (Cary5000) and photoluminescence spectrophotometer from SHIMADZU (RF-530 Spectrofluorophotometer).

#### 2.5 Cell testing

The current density–voltage ( $J-V$ ) characteristics of the fabricated cells were recorded by using a Keithley 2400 Source Meter under simulated sunlight using a SS50AAA (Photo Emission Tech) solar simulator at AM 1.5G ( $100 \text{ mW cm}^{-2}$ ). The active area of the cell was controlled to be  $0.25 \text{ cm}^2$  for all the cells.

### 3. Results and discussion

#### 3.1 Structural analysis

The XRD patterns of ITO substrate and TGR nanocomposite films with varying concentrations of graphene from 0 to 1 wt% are shown in figure 2. It shows that the TGR nanocomposites with different weight addition ratios of graphene display like

XRD patterns. The peaks at  $2\theta$  values of  $25.2^\circ$ ,  $37.8^\circ$ ,  $48.0^\circ$ ,  $53.9^\circ$  and  $55.1^\circ$  can be assigned to (101), (004), (200), (105) and (211) crystal planes of anatase  $\text{TiO}_2$ , respectively [14]. The typical diffraction peak belonging to the graphene in TGR nanocomposites was observed at  $2\theta$  value of  $26.8^\circ$  [20] and intensity of this peak keep increasing as the concentration of graphene in the nanocomposites increases. No other impurity peaks were observed confirming the purity of the samples.

#### 3.2 Morphological analysis

The surface morphology of TGR nanocomposite films coated on the ITO surface are examined using FESEM. Typical FESEM micrographs of TGR 0, TGR 0.25 and TGR 1 nanocomposite films are shown in figure 3. It can be seen from these micrographs that these films are rougher and have porous morphology as compared to TGR 0. The

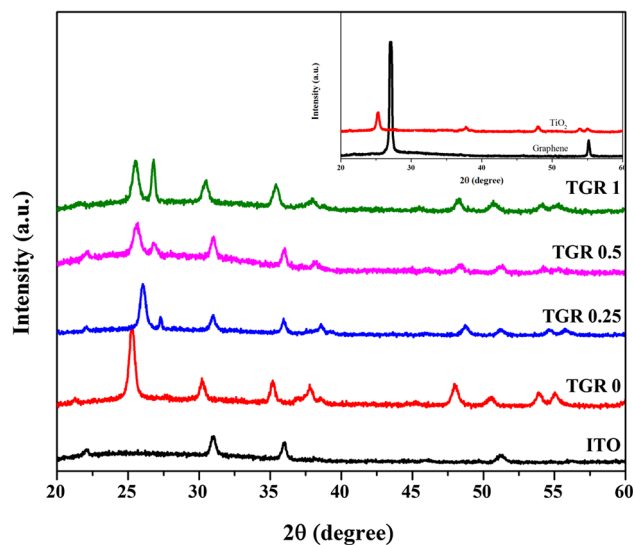


**Figure 2.** XRD patterns of ITO substrate and TGR nanocomposite films. Inset of the figure shows XRD patterns of  $\text{TiO}_2$  and graphene powders.

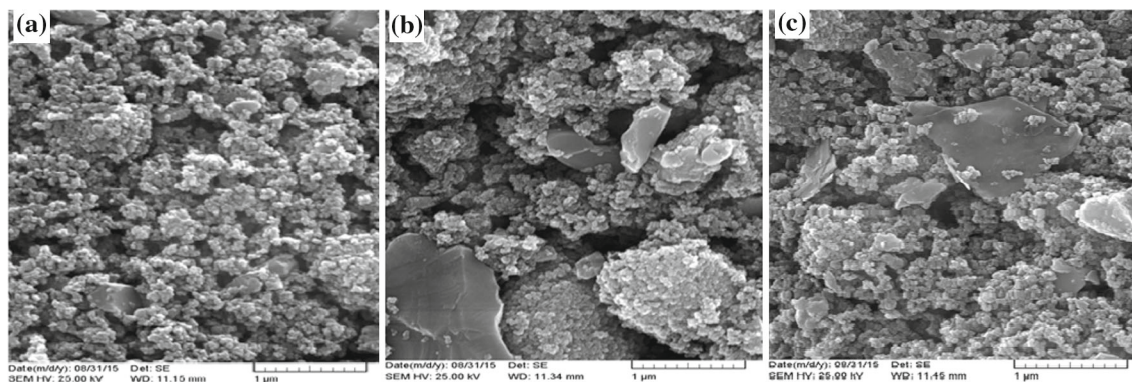


**Figure 3.** Typical SEM micrograph of (a) TGR 0, (b) TGR 0.25 and (c) TGR 1 nanocomposite films.

porosity and the average pore size of these films are calculated by using ImageJ (v. 1.48) software [29] and the values are summarized in table 1. The table shows that the porosity of these films goes on increasing as the graphene content increases in these nanocomposites. It means that the insertion of graphene made more porous photoanode film. Because of its 2D structure, graphene could lead to more effective separation than 1D structured carbon nanotubes (CNTs). It has been reported by Eshaghi *et al* [30] that more porous films are capable of adsorbing more dye, thereby enhancing the efficiency of DSSCs. But further increase in porosity facilitates the electrolyte to permeate into porous network and causes recombination [31,32].

### 3.3 Compositional analysis

The typical EDX spectrum of TGR 0, TGR 0.25 and TGR 1 nanocomposite photoanode films are shown in figure 4. Carbon peak in these TGR nanocomposites can be easily seen which confirms the presence of graphene in the TiO<sub>2</sub> matrix. The gold (Au) coating was done prior to the EDX measurement; therefore, spectrum also contains peaks of Au.

### 3.4 Optical studies

3.4a *UV-visible absorption spectra:* Varying concentrations of graphene present in TGR nanocomposites considerably affect the light absorption. Generally, the pure TiO<sub>2</sub> shows

no absorption over its fundamental absorption edge (around 400 nm). In contrast, the TGR nanocomposites exhibit enhanced absorption in the visible region [33] as shown in figure 5. In addition, the absorption edge of TGR 0.25, TGR 0.5 and TGR 1 nanocomposites are shifted towards higher wavelength region; hence, pointing towards narrowing of band gaps attributed to the formation of chemical bonds between TiO<sub>2</sub> and graphene such as Ti–O–C [34]. As the extended absorption towards visible region is understood to be due to contribution from graphene; therefore, these nanocomposites utilize the solar spectrum more efficiently as compared to TGR 0 and show a significant enhancement in the photoconversion efficiency of DSSCs [35]. The band gap of all the TGR nanocomposites films is calculated using the Tauc Law [36]:

$$\alpha h\nu = \text{const}(h\nu - E_g)^2.$$

Here  $E_g$  is the optical band gap and  $\alpha$  is calculated as  $2.303A/d$ ,  $d$  being the thickness of the sample and  $A$  is the optical density. Thickness of all the samples was found to be 9  $\mu\text{m}$  as measured by digital micrometer screw gauge with least count of 1  $\mu\text{m}$ . The Tauc plots of all TGR nanocomposites are shown in figure 6. The band gaps are obtained by extrapolating the linear portion of the curve to the abscissa. The band gap values of TGR 0, TGR 0.25, TGR 0.5 and TGR 1 were found to be 3.24, 2.78, 3.11 and 3.19 eV, respectively. In semiconductors, band gaps are directly related to the range of wavelength absorbed specifically; band gap decreases with the increase in absorption wavelength and the present results are in accordance with the literature reported previously [37]. The layers of molecules can slip on one another in the graphene structure that makes it a conducting material; therefore, incorporation of graphene in TiO<sub>2</sub> network may lead a hike in DSSCs efficiency value. TGR 0.25 has the lowest maxima in UV region, but its overall absorption was increased in visible region (figure 5) as compared to other nanocomposite

**Table 1.** Porosity and average pore size of TGR nanocomposite films.

Sample	Porous area, %	Average pore size, $\mu\text{m}$
TGR 0	18.117	0.256
TGR 0.25	22.364	0.408
TGR 1	25.161	0.274

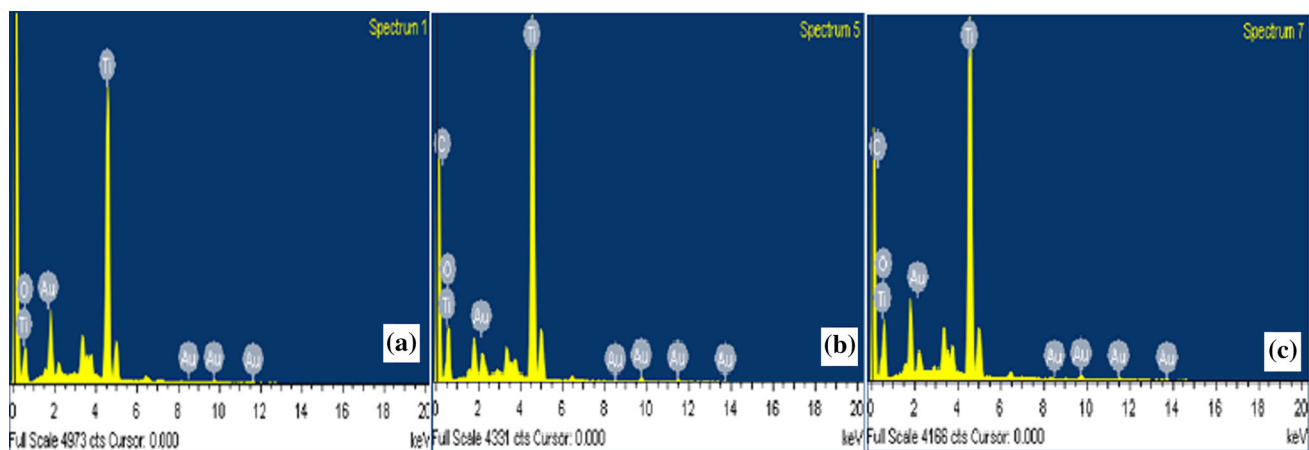


**Figure 4.** Typical EDX spectrum of (a) TGR 0, (b) TGR 0.25 and (c) TGR 1 nanocomposite films.



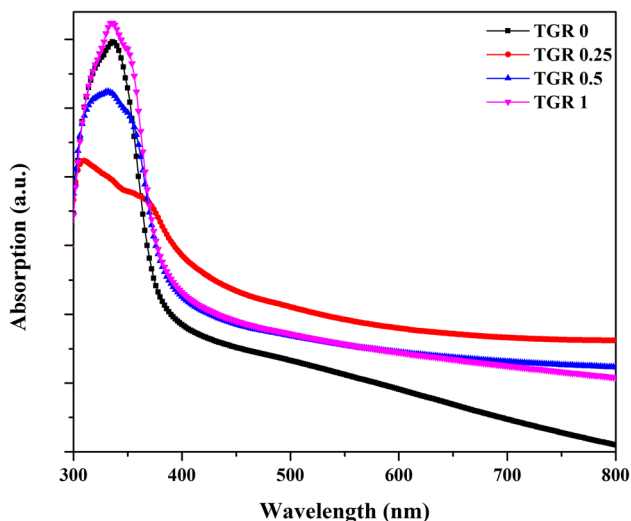


**Figure 5.** UV-visible absorption spectra of TGR nanocomposite films.

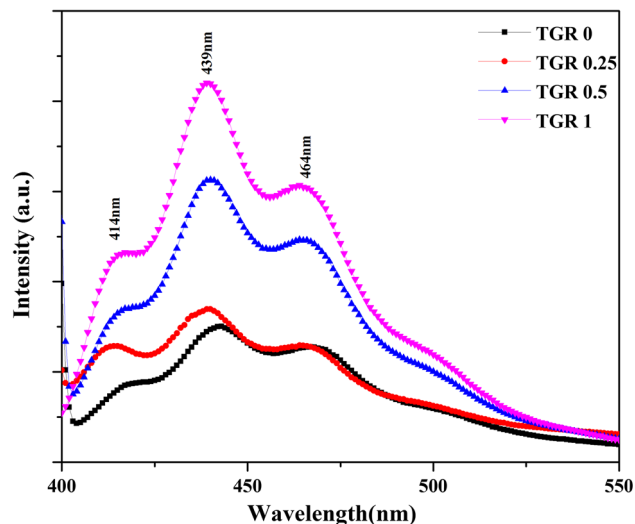


**Figure 7.** PL spectra of TGR nanocomposite films.

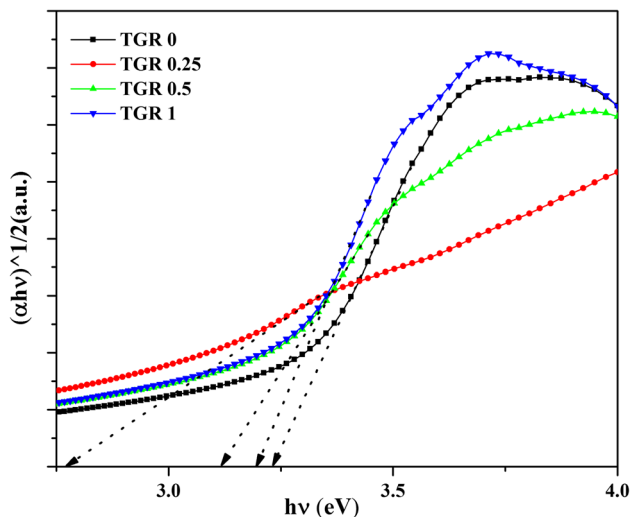


**Figure 6.** Tauc plots of TGR nanocomposite films.

films. Tauc plots indicate that TGR 0.25 has the least band gap among all the prepared nanocomposites, which supports a favourable electron injection process as compared to other competitors. Doping of high concentration of graphene in  $\text{TiO}_2$  layer may hinder the transport phenomenon through it.

**3.4b PL spectra:** As the study of photoluminescence (PL) spectra helps to unveil the performance of charge carrier trapping, separation as well as to make out the fate of excitons in semiconductor materials, because PL emission arises due to the recombination of photogenerated charge carriers. Therefore, a room temperature PL spectrum of TGR nanocomposite photoanode films (at excitation wavelength of 380 nm) is

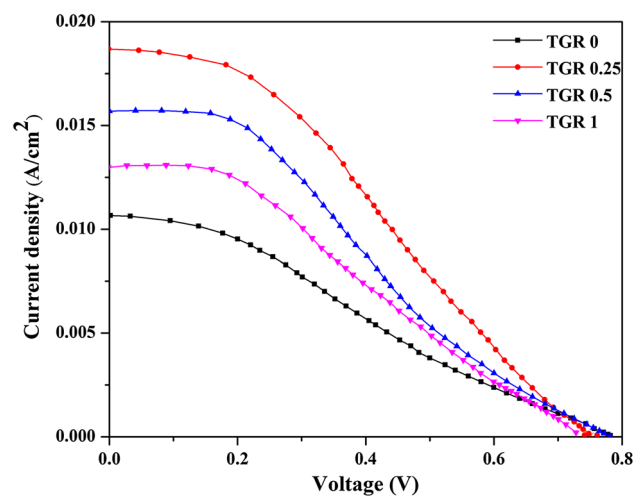


**Figure 8.**  $J$ - $V$  curves of TGR nanocomposite films based DSSCs.

recorded and is shown in figure 7. All the samples show three emission peaks situated at  $\sim 415$ , 439 and 464 nm, respectively, owing to band-band emission in addition to metal-ligand charge transfer transition [38,39]. PL intensity varies in the order of TGR 1 > TGR 0.5 > TGR 0.25. This order is in well agreement with the expected results as the PL intensity increases, if the surface becomes less transparent because incorporation of more and more graphene increases the opacity of the  $\text{TiO}_2$  films and consequently enhances PL intensity.

### 3.5 Photocurrent density-voltage characteristics

Figure 8 shows typical density-voltage ( $J$ - $V$ ) curves acquired from DSSCs fabricated with different TGR nanocomposites (0–1 wt%), photoanode films with active area of  $0.25 \text{ cm}^2$  using solar simulator with AM 1.5G ( $100 \text{ mW cm}^{-2}$ ).

**Table 2.** Photovoltaic performance of DSSCs calculated from  $J-V$  curves with TGR nanocomposite photoanodes.

Sample	$J_{SC}$ , mA cm <sup>-2</sup>	$V_{OC}$ , V	FF	$\eta$ , %
TGR 0	10.4	0.78	0.29	2.35
TGR 0.25	18.4	0.75	0.34	4.69
TGR 0.5	15.6	0.77	0.30	3.60
TGR 1	12.8	0.73	0.29	2.71

Different parameters such as photocurrent density ( $J_{SC}$ ), open circuit voltage ( $V_{OC}$ ), fill factor (FF) and efficiency ( $\eta$ ) obtained from these curves are summarized in table 2. It can be seen from this table that an increase in  $J_{SC}$  and  $\eta$  is observed in DSSCs made with TGR 0.25 as compared to TGR 0. The optimum porosity, optimum conductance, least band gap and least PL emission make TGR 0.25 as a good candidate among all the samples under study. Efficiency decreases with high concentration of graphene; for example, TGR 1 which may be attributed due to the decrease in active TiO<sub>2</sub> sites available for electron transfer [40]. Further work is going on for the optimization of DSSC parameters for the fabrication of this device with enhanced efficiency.

#### 4. Conclusions

The study of efficiency value reveals that the TGR nanocomposites (0.25–1 wt%) films are better candidates as compared to TGR 0 photoanode, since graphene reduces loss of electrons and their recombinations. The incorporation of graphene makes the films more opaque favouring the trapping of light within the TiO<sub>2</sub> network and increasing the efficiency. Conducting nature of graphene helps in a better transportation of electrons in the operating mechanism of a DSSC. It is observed that if graphene content is increased beyond 0.25 wt%, morphology becomes more porous, which makes a way for electrolyte to reach TiO<sub>2</sub> layer and cause recombination, thereby reducing photocurrent. The highest efficiency of 4.69% of the device was obtained with TGR 0.25 nanocomposite photoanode under full sunlight of 100 mW cm<sup>-2</sup> with AM 1.5G conditions. This efficiency value with low-cost materials is a good sign in the field of DSSCs that aims at cost-wise efficiency.

#### Acknowledgements

We are grateful to UGC-SAP (DRS-II), Department of Physics, Delhi University (New Delhi) and IUAC (an autonomous centre of UGC) for providing the facilities of XRD,  $J-V$  characteristics and FESEM with EDX, respectively.

#### References

- [1] Oregan B and Grätzel M 1991 *Nature* **353** 737
- [2] Moula G, Mumin M A and Charpentier P A 2013 *J. Nanomater. Mol. Nanotechnol.* **S1** 1
- [3] Kay A and Grätzel M 1996 *Sol. Energy Mater. Sol. Cells* **44** 99
- [4] Chiba Y, Islam A, Watanabe Y, Komiya R, Koide N and Han L 2006 *Jpn. J. Appl. Phys.* **45** L638
- [5] Kaur M and Verma N K 2013 *J. Mater. Sci.: Mater. Electron* **24** 1121
- [6] Jyoti D, Mohan D and Dhar R 2013 *J. Renew. Sustain. Energy* **5** 013112
- [7] Grätzel M 2001 *Nature* **414** 338
- [8] Tsai T H, Chiou S C and Chen S M 2011 *Int. J. Electrochem. Sci.* **6** 3333
- [9] Zhu K, Neale N R, Miedaner A and Frank A J 2007 *Nano Lett.* **7** 69
- [10] Lee Y and Kang M 2010 *Mater. Chem. Phys.* **122** 284
- [11] Ma H, Tian J, Cui L, Liu Y, Bai S, Chen H et al 2015 *J. Mater. Chem. A* **3** 8890
- [12] Song C B, Qiang Y H, Zhao Y L, Gu X Q, Zhu L, Song J et al 2014 *Int. J. Electrochem. Sci.* **9** 8090
- [13] Qu J and Lai C 2013 *J. Nanomater.* <https://doi.org/10.1155/2013/762730>
- [14] Zhang Y, Tang Z R, Fu X and Xu Y J 2010 *ACS Nano* **4** 7303
- [15] Geim A K and Novoselov K S 2007 *Nat. Mater.* **6** 183
- [16] Allen M J, Tung V C and Kaner R B 2010 *Chem. Rev.* **110** 132
- [17] Stankovich S, Dikin D A, Dommett G H B, Kohlhaas K M, Zimney E J, Stach E A et al 2006 *Nature* **442** 282
- [18] Geim A K 2009 *Science* **324** 1530
- [19] Mohamed R M 2012 *Desalin. Water Treat.* **50** 147
- [20] Stengl V, Bakardjieva S, Grygar T M, Bludaska J and Kormunda M 2013 *Chem. Central J.* **7** 1
- [21] Jyoti D, Mohan D and Dhar R 2012 *Modern Phys. Lett. B* **26** 1250123
- [22] Jyoti D, Mohan D, Dhar R and Singh A 2012 *Invertis J. Renew. Energy* **2** 29
- [23] Gaya U I and Abdullah A H 2008 *J. Photochem. Photobiol. C: Photochem. Rev.* **9** 1
- [24] Kim A Y, Kim J, Kim M Y, Ha S W, Tien N T T and Kang M 2012 *Bull. Korean Chem. Soc.* **33** 3355
- [25] Zhang N, Zhang Y and Xu Y J 2012 *Nanoscale* **4** 5792
- [26] Yang N, Zhai J, Wang D, Chen Y and Jiang L 2010 *ACS Nano* **4** 887
- [27] Tan L L, Ong W J, Chai S P and Mohamed A R 2013 *Nanoscale Res. Lett.* **8** 1
- [28] Lim S P, Pandikumar A, Huang N M and Lim H N 2015 *Int. J. Energy Res.* **39** 812
- [29] Abramoff M D, Magalhães P J and Ram S J 2004 *Biophotonics Int.* **11** 36
- [30] Eshaghi A and Aghaei A A 2015 *Bull. Mater. Sci.* **38** 1177
- [31] Jyoti D, Mohan D and Singh A 2014 *Int. J. Enhanced Res. Sci. Technol. Eng.* **3** 388
- [32] Jyoti D and Mohan D 2012 *Int. J. Sci., Eng. Comp. Technol.* **2** 83
- [33] Liu S, Liu C, Wang W, Cheng B and Yu J 2012 *Nanoscale* **4** 3193
- [34] Huang Q, Tian S, Zeng D, Wang X, Song W, Li Y et al 2013 *ACS Catal.* **3** 1477

- [35] Lu T, Zhang R, Hu C, Chen F, Duo S and Hub Q 2013 *Phys. Chem. Chem. Phys.* **15** 12963
- [36] Tauc J, Grigorovici R and Vancu A 1966 *Phys. Status Solidi* **15** 627
- [37] Kazmi S A, Hameed S, Ahmed A S, Arshad M and Azam A 2017 *J. Alloys Compd.* **691** 659
- [38] Sadhu S and Poddar P 2014 *J. Phys. Chem. C* **118** 19363
- [39] Jin C, Liu B, Lei Z and Sun J 2015 *Nanoscale Res. Lett.* <https://doi.org/10.1186/s11671-015-0790-x>
- [40] Madhavan A A, Ranjusha R, Daya K C, Arun T A, Praveen P, Sanosh K P *et al* 2014 *Sci. Adv. Mater.* **6** 1